Liquid Metal Magnetohydrodynamic Pump for Junction Temperature Control of Power Modules

Y. Yerasimou, V. Pickert, MIEEE, X. Song, B. Ji, MIEEE

Abstract— **Power modules are the most common components to fail in power converters that are employed in mass transportation systems, thus leading to high unscheduled maintenance cost. While operating, high junction temperature swings occur that result in high thermomechanical stress within the structure of the power module reducing the lifetime of the module. Liquid metals as a cooling medium received so far little attention in the area of power semiconductors cooling, despite being able to remove high heat fluxes. This paper shows for the first time how liquid metal is used to reduce actively the junction temperature swing. A magnetohydrodynamic (MHD) pump has been designed for this purpose allowing active control of the flow rate of the liquid metal that impinges against the baseplate of the module. The pump has been 3D printed and forms with the power module a unique unit. A closed-loop temperature control system is implemented, able to estimate the IGBT's junction temperature and thus, control the MHD power. The paper presents simulation and experimental results showing reductions in the temperature swing over the full load cycle with 12°C as the highest observed reduction rate. The paper shows also detailed designs of the MHD pump and the controller hardware.**

Index Terms — **IGBT power module cooling, reliability, liquid metal cooling, magnetohydrodynamic pump, junction temperature**

I. Introduction

APPLICATIONS such as offshore wind power, subsea drilling and railway, require power converter systems that demonstrate high life spans, as cost for unscheduled maintenances can be extremely high for these applications. Many components, such as power semiconductor modules [1], capacitors [2], and printed circuit boards (PCBs) [3] are reliability critical for the power converter operation. This study focuses on increasing the lifetime of power semiconductor devices. A lifetime model for estimating the cycles to failure of a power semiconductor module was developed in the 90s by the LESIT research program [4]. In that program the number of cycle to failure (N_f) for a power module is expressed as a function of its working conditions, such as the junction temperature swing (ΔT_j) and the mean junction temperature (T_m), as shown in (1):

$$N_f = a \cdot (\Delta T_j)^{-n} \cdot e^{E_a/(k_B \cdot T_m)} \tag{1}$$

where a and n are material dependent coefficients, E_a is the activation energy and k_B is the Boltzmann constant. The outcomes of the LESIT study are illustrated in Fig. 1 [4], clearly showing that the most influencing factor for power modules failures is ΔT_j. Reducing the temperature fluctuations, even at the cost of operating at a higher mean temperature, could dramatically increase the lifespan of IGBT power modules. Further research has shown that the lifetime of power electronic modules depends on many other parameters, including the pulse duration, the current amplitude and other packaging parameters, however, the dominant factor for power electronic failures remains the junction temperature swing, ΔT_j [5].

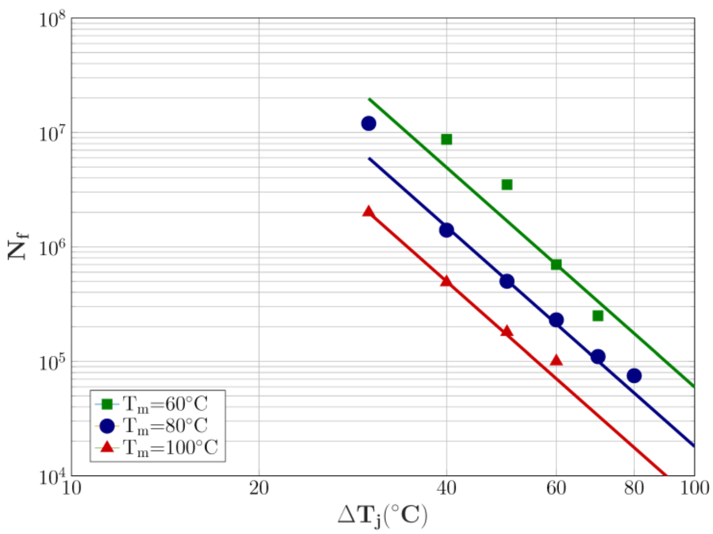

Fig. 1. Power cycling results from LESIT project, showing the dependency of power modules lifespan N_f on junction mean temperature T_m and junction temperature swing ΔT_j [4].

Fig. 2 shows the schematic of a common power module. Its structure consists of many layers of different materials, each one owning a different coefficient of thermal expansion (CTE). During large temperature fluctuations, a shear force is generated between the layers because of the mismatch in the CTE of the power module's materials. Hence, the thermomechanical stress within the layers consequently leads to devices' failures such as bond wire lift-off [6] and solder joint fatigue [7]. Thus, reducing temperature fluctuations by reducing the amplitude of ΔT_j can prolong the lifetime of power modules and reduce the possibility of a failure [8].

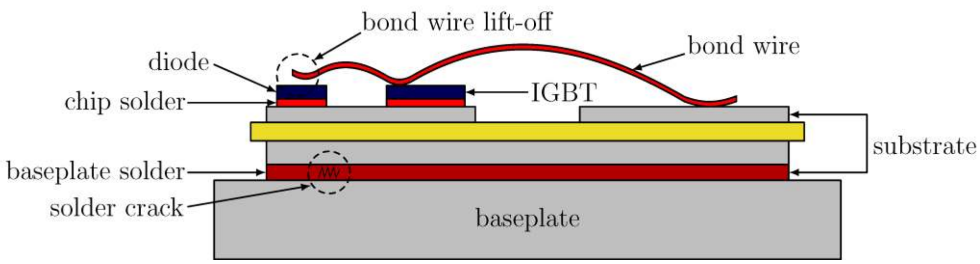

Fig. 2. Typical power module structure

In order to keep power semiconductors below the maximum allowable operating temperature, water is widely used as a cooling medium. Most commonly, water pipes are routed in a cold plate in a meander structure [9]. In recent years, research has been focused on further enhancing liquid cooling effectiveness by introducing techniques, such as micro/mini-channel based heat sinks, impingement based techniques and two-phase cooling, to meet the cooling requirements of high power-dense power electronics [10-14]. Lately, liquid metals have been introduced as coolants, as they have a much higher thermal conductivity compared to water. The design, development and fabrication process of an magnetohydrodynamic (MHD) pump has been reported for a few cooling applications, such as cooling high-performance CPUs [15-17], high-power light emitting diodes [18], high-power laser diodes [19], and power switching modules [20, 21]. In all of these applications, MHD pumps were operated at constant power to protect the power module from thermal runaway. In addition, in the previous examples the liquid metal is contained within the pipes of the cooling system. Hence, the excess heat is dissipated without the coolant contacting the baseplate of the power module directly, which introduces additional resistance for the thermal path. The implementation of an adaptive forced-air cooled heat sink was presented in [22] and [23], demonstrating an increase in the lifetime of power electronic devices through power cycling tests. Nonetheless, with the ever-increasing power densities of power electronics, air-cooled technologies are unable to dissipate the excess heat [9]. In addition, an adaptive thermoelectric cooling (TEC) was presented in [24]. However, as TECs need to dissipate the heat that is being moved from the semiconductor chip and the heat that is generated from its own power, their heat dissipation capability is limited [25].

This paper presents for the first time the design, development and implementation of an MHD-driven, liquid metal heat sink that can be used for cooling and for actively reducing the amplitude of the junction temperature cycle of an Insulated Gate Bipolar Transistor (IGBT) power module through active control of the junction temperature. Moreover, the pump is integrated to the power module and impinges liquid metal to its baseplate directly, thus reducing the overall thermal resistance of the system by eliminating the need for thermal grease.

The paper is structured as follows: Section II introduces the principal methodology and the control structure to reduce the junction temperature swing and shows simulation results. Section III describes the liquid metal MHD pump design that has been used in the experiment. The experimental test set-up is described in Section IV. Experimental results demonstrating reduction in temperature variations are shown in Section V. Section VI concludes the work.

II. Principal Methodology and Control Structure

A. Time-dependent Thermal Cycles of Power Modules

In real applications, the temperature profile of power semiconductors is jointly determined by operating and environmental conditions, whose dynamic changes in terms of time constants generally shows diverse differences, as shown in Fig. 3. The time constants governing the device and circuit electrical properties usually range from sub-microseconds to milliseconds and are related to the characteristic performance of the switching device and switching frequency of the power converter. Similarly, the time constant of a mechanical system typically including the motor drive, shaft and mechanical load could vary from sub-seconds to several minutes. Finally, the long term thermal cycle is associated with environmental changes, such as the day-night and seasonal alternation-driven temperature variation or geographical/spacious relocation- driven temperature changes. Power modules are subjected to cyclic thermomechanical stresses resulted from the superposed temperature deviations mentioned above. Power modules are mostly stressed because of load changes with regards to the mechanical system requirement, which is always accompanied by large temperature swings occurring at a substantial frequency [18]. Changes associated with environmental temperature contribute to the module ageing, however, they are outperformed by the load cycling [26]. On the other hand, temperature cycles caused by the device switching action and circuit topological alternations result in very small amplitude that does not greatly impact the lifetime of a healthy power semiconductor module [27]. That is partly because the thermal variation caused by higher frequencies is counterbalanced by the capacitance of the thermal circuit, and partly because the thermal strain is counterbalanced by the elastic deformation of the power module's materials.

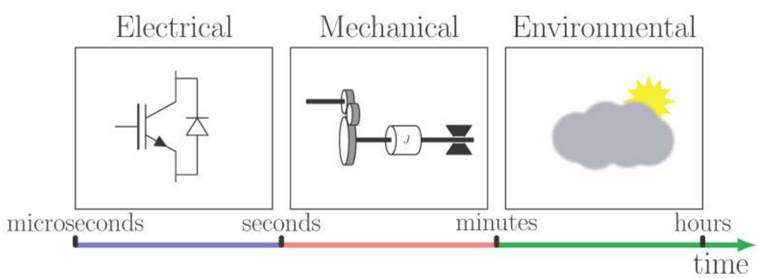

(a)

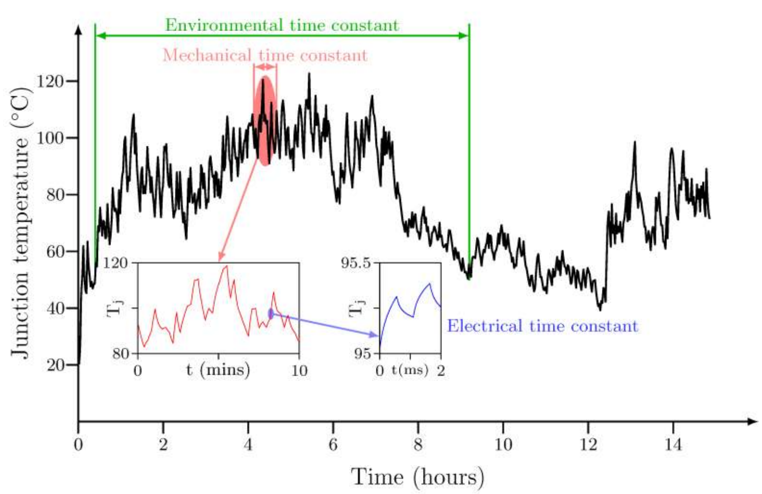

(b)

Fig. 3. Typical variations of junction temperature during operation: (a) time constants of various thermal cycles during power semiconductor operation and (b) example temperature profile showing the different time constants

B. Enable Proactive Thermal Management using Adaptive Heatsink

In order to reduce the significant thermal cycles dominated by load changes in the mechanical time constant range, an adaptive heat sink can be designed to offset the temperature variations by adjusting its inherent cooling performance. This will then reduce the module's fatigue and therefore, increase the lifetime of power semiconductor devices. The proposed temperature control scheme is achieved by employing an actively controlled liquid metal heat sink enabled by an MHD pump that changes the coolant's flow rate in terms of the change of the junction temperature (T_j).

Fig. 4(a) shows a typical Cauer thermal network of an IGBT power module cooled by a water cooling heat sink, where the cold plate is emulated by the n_{th} node of the resistance - capacitance (*RC*) ladder. The Cauer network has a physical basis, as each *RC* element represents a physical layer of the module. These *RC* networks are constant and Fig. 4(a) assumes that all of the heat produced in the semiconductor chip travels through all module layers into the coolant. As the total thermal resistance is fixed, the junction temperature becomes only a function of power losses ($P_{(t)}$) and the water temperature (T_{water}). In comparison, in Fig. 4(b) the water cold plate is replaced by an active liquid metal heatsink powered by the MHD pump, which is positioned directly under the base plate to achieve a small form factor by integrating the MHD pump with the heat sink. The thermal resistance (R_{thn}) of the new heat sink is adjustable and as demonstrated in [28], and the value of R_{thn} is a function of the liquid metal flow rate (Q). The variable thermal resistor is controlled in such a way that it is changing the cooling rate in order to minimize ΔT_j. Similarly, T_{lm} represents the liquid metal's inlet temperature.

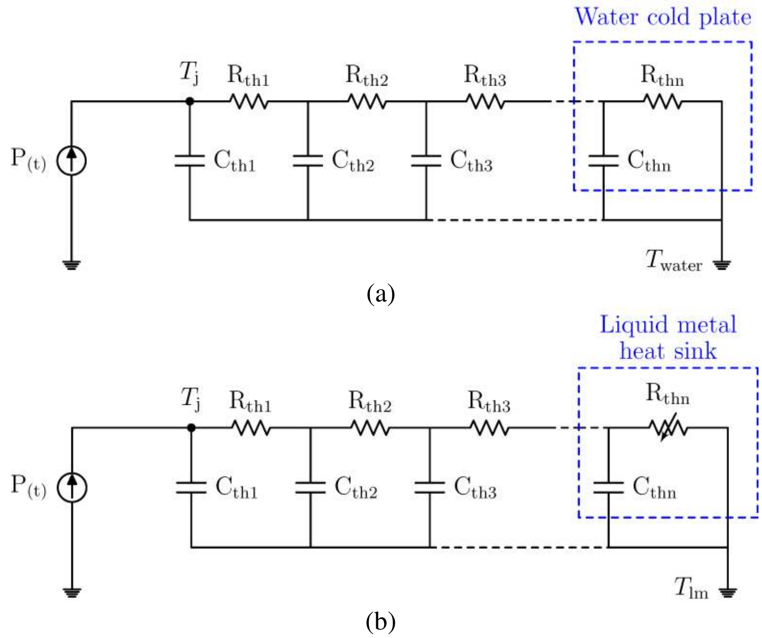

Fig. 4. Equivalent thermal network for IGBT with (a) water cooled cold plate and (b) adaptive liquid metal MHD cooling

C. Comparison of Thermal Networks and their Cooling Capabilities

An 8^{th} order Cauer thermal network was developed for simulating the junction temperature of an IGBT die in a power semiconductor module, where the first 7 Cauer elements represent the IGBT device and the 8^{th} element emulates the liquid metal MHD pump. Fig. 5 shows the schematic of the circuit including the principal control structure, which was simulated in PLECS. The losses of the IGBT switch are emulated by an input signal that is fed to the power source, $P_{(t)}$. The junction temperature is compared to a reference temperature and the error between those two values is fed to a proportional controller. Hence, the value of the variable thermal resistance is changed based on the instantaneous IGBT junction temperature, in order to reduce the junction temperature fluctuation, ΔT_j. A proportional controller was selected, as the proposed scheme considers temperature changes dominated by the mechanical system of a relatively large time constant. The gain value (k_p = 0.2) is selected based on the overall thermal resistance boundaries of the system. Table I shows the thermal parameters of the IGBT module that is used for the experiment (SEMIKRON SKM 50GB063D), which were extracted from [29]. The traditionally used thermal grease layer is omitted due to the direct interface between the module and the liquid metal. The experimental results in [20] have demonstrated a thermal resistance of 0.094 °C/W for a liquid metal heatsink used in a power electronics cooling application. The maximum thermal resistance limit of 3 °C/W was obtained empirically. Hence, the thermal resistance R_{th8} is set between 0.094 °C/W and 3 °C/W, where the liquid metal flow rate is maximum at the minimum thermal resistance limit and zero at the maximum thermal resistance limit.

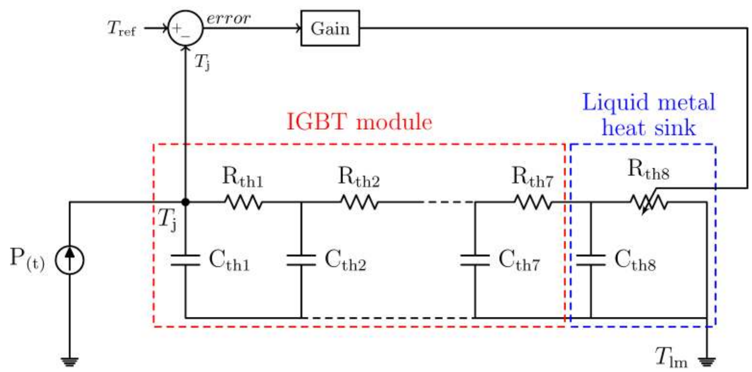

Fig. 5. Simulation schematic of IGBT temperature control scheme.

Power modules used in electric rail traction applications are expected to have at least 30 years of reliable operation that corresponds to several millions of power cycles [30], therefore, a metro-system mission profile was selected for this study [31]. A repeating cycle that consists of the following steps was applied to the simulation model: accelerating for 41 s, travelling at 60 km/h for 37 s, braking for 10 s, travelling at 40 km/h

TABLE I
THERMAL PARAMETERS FOR POWER SEMICONDUCTOR DEVICE AND LIQUID METAL MHD PUMP

Material	Cauer node	Thermal resistance (°C/W)	Thermal capacitance (J/°C)
Silicon die	1	0.0319	0.015
Die attach	2	0.037	0.0047
Copper	3	0.0155	0.05
Aluminum oxide	4	0.2411	0.078
Copper	5	0.0108	0.072
DCB solder	6	0.0211	0.0082
Baseplate	7	0.054	1.394
Liquid metal heat sink	8	0.094 – 3	50

for 11 s, braking for 22 s and finally, making a complete stop for 30 s. The original mission profile is scaled down, with the maximum load current capped to 50 A to meet the requirements of the selected IGBT module (the maximum current used later in the experiment is also limited to 50 A). The simulation results are presented in Fig. 6. The scaled down mission profile has been converted into a simplified power loss profile $P_{(t)}$ that accounts only for the on-state losses, as shown in Fig. 6(a). Based on the actual junction temperature

T_j variation and the reference temperature T_{ref}=50°C the controller minimizes temperature swings ΔT_j by manipulating the thermal resistance R_{th8}. The change of R_{th8} over time is shown in Fig. 6(b). It is shown that R_{th8} decrease with rising $P_{(t)}$, and vice versa. During the stop mode of the metro, the MHD pump is commanded to stop pumping liquid metal resulting in a constant high value of R_{th8}=3°C/W during this period, whereas a minimum thermal resistance is required during dynamic accelerating/braking.

Adaptive cooling intends to mitigate the thermal stresses compared to the constant cooling based on the comparison of the junction temperatures T_j evolution over the full mission profile. Fixing R_{th8} represents the use of a cold plate with constant flow rate and this scenario can therefore be regarded as a standard cold plate as shown in Fig. 4(a). The thermal resistance value for the latter simulation was set to its lowest value of R_{th8}=0.094°C/W. Fig. 6(c) shows an evident impact on ΔT_j reduction for an adjustable R_{th8}. Particularly, both the maximum junction temperature swing and the frequency of ΔT_j swing with large amplitude are reduced. Over the full metro mission profile, ΔT_j of the adaptive cooling is much smaller compared to ΔT_j of constant cooling. The adaptive cooler achieves its highest temperature swing reduction during the acceleration from standstill to maximum speed. In this mode the junction temperature changes by 18°C using the controlled MHD pump compared to 33°C when uncontrolled. This is nearly a 50% reduction in temperature swing. Fig. 6(c) shows that the mean junction temperature T_m of the adaptive cooling is 44°C and 35°C for the cold plate with fixed R_{th8}. The rise in the mean temperature is the result of the tighter control of the junction temperature. The uncontrolled cold plate produces more frequent and longer colder junction temperatures over time which in average brings down the mean junction temperature value. In spite of the higher mean junction temperature of the device while T_j is actively controlled, the thermal stress within the module's layers is reduced.

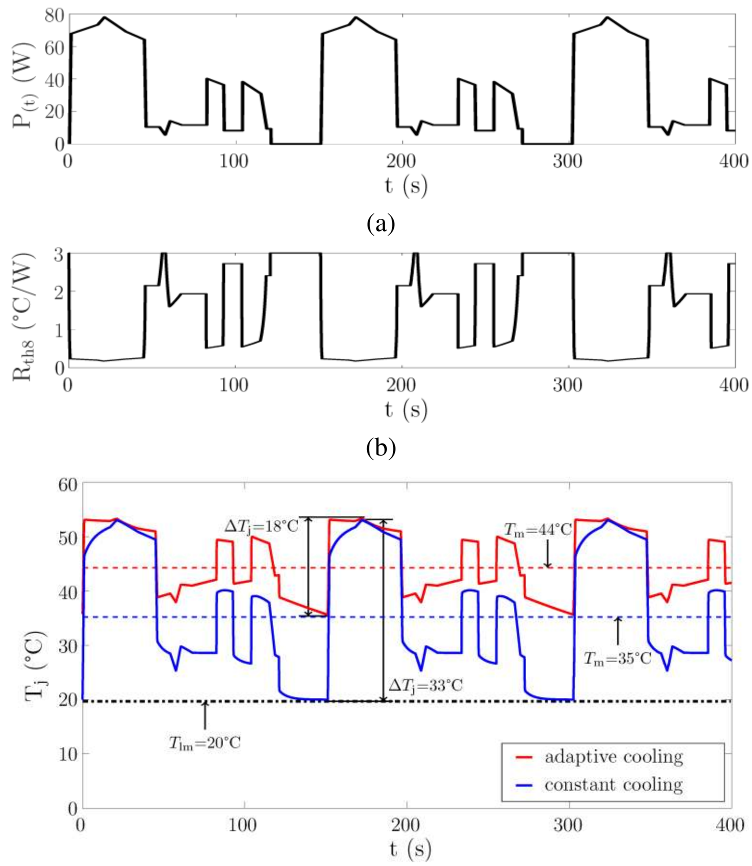

(c)

Fig. 6. Simulation results for metro mission profile showing, (a) input heat profile $P_{(t)}$, (b) variation of the thermal resistance R_{th8} and (c) junction temperature T_j for constant and adaptive cooling.

The simulated temperature control scheme relies on accurate junction temperature measurement, however, implementing a temperature estimation technique in the real design is not a trivial task. In this work, a Temperature Sensitive Electrical Parameter (TSEP) is employed for sensing T_j and it is discussed in detail in Section IV. In addition, the thermal resistance of the active heat sink is adjusted instantly in line with the changing junction temperature, which is not the case for the proposed liquid metal heat sink, as the thermal resistance is associated with the liquid metal flow rate and therefore, a certain period of time is required before it reaches steady state. Hence, time delays that might occur during the variation of the liquid metal flow rate have not been taken into consideration for the simulation but will be discussed in the experimental setup.

III. Liquid Metal MHD Pump

A. Active Heat Sink Structure

The self-contained liquid cooling system consists of two parts; a MHD pump head with direct immersion cooling and a U-type tubular liquid metal-to-water heat exchanger with connection pipes. Fig. 7 shows the schematic drawing and the implementation of the cooling system. The SEMIKRON SKM 50GB063D is used as the device-under-test (DUT). The DUT is bolt on the pump head and there is a direct interface between the backside of the baseplate and the liquid metal coolant. The coolant flowing is confined to the designed liquid block and directed by two narrow slots in the Nylon housing, as shown in Fig. 8(a). The liquid block is sealed with an o-ring. The heat source is in direct contact with the liquid metal which impinges the baseplate as illustrated by Fig. 8(b). The U-type heat exchanger and the pump head are connected with two short pipes to form a closed loop. The pump is positioned beneath one IGBT chip of the half bridge module, as this is the only one used in the experiment. The 3D printed housing of the pump head is made of engineering plastic (VeroWhite™), which is able to provide good electrical insulation, good waterproofness, good chemical resistance and sufficient rigidity. The main disadvantage of the selected material is its relatively low glass transition temperature T_g, which equals 52ºC. That is the point at which the material transitions from hard to soft. The 3D printed material is utilized in this study to demonstrate the effectiveness of the proposed heat sink in reducing the temperature fluctuation of T_j in a laboratory environment, however, for a real-case application, a material with a higher T_g should be selected.

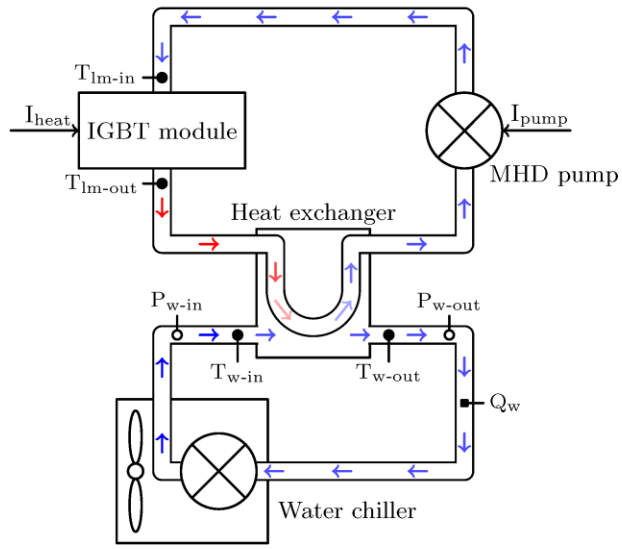

Fig. 7. Schematic diagram of the cooling circuit.

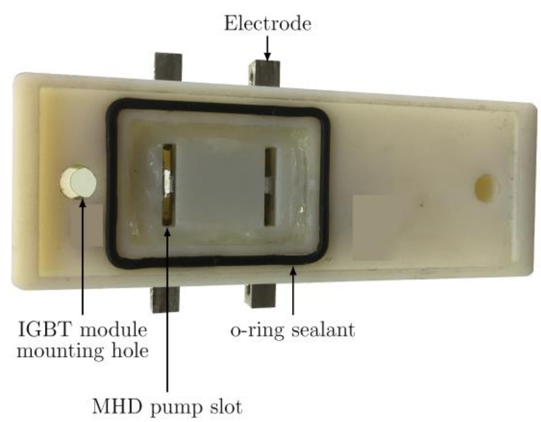

(a)

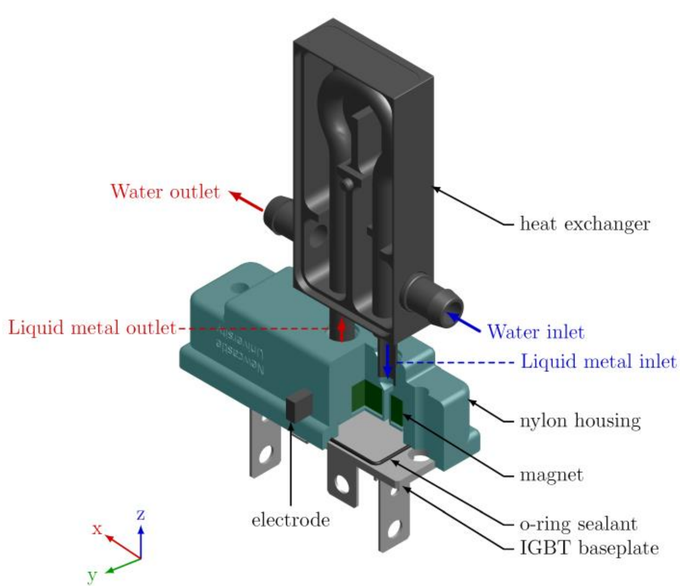

(b)

Fig. 8. Detailed view of the active liquid metal cooler: (a) bottom view of the cooler and (b) isometric view of the cooler and IGBT module.

B. Construction of the MHD Pump

Two MHD micro-pumps are integrated in the plastic housing, where totally five magnets are embedded in ***x*** direction and a pair of nickel electrodes is embedded in ***y*** direction and thus, perpendicular to the magnets. The coolant used for this application is the eutectic alloy $Ga_{68}In_{22}Sn_{10}$ (68% Ga, 22% In and 10% Sn). It has a similar composition to Galinstan™ and its thermophysical properties are shown in Table II. Compared to water, which is widely used as a cooling medium for power electronic applications, $Ga_{68}In_{22}Sn_{10}$ has a much lower specific heat capacity (C_p). Hence, its volumetric heat capacity ($C_v=\rho\cdot C_p$) is about 55% lower compared to water's volumetric heat capacity. Nonetheless, $Ga_{68}In_{22}Sn_{10}$ has a higher cooling capability due to its high thermal conductivity, which is approximately 27.2 times larger than water's thermal conductivity.

TABLE II
THERMOPHYSICAL PROPERTIES OF LIQUID METAL AND WATER

Property	Unit	Water	$Ga_{68}In_{22}Sn_{10}$
Density	kg/m^3	998	6400
Melting point	°C	0	-19
Boiling point	°C	100	>1300
Specific heat capacity	J/(kg·°C)	4181	365
Dynamic viscosity	Pa·s	0.001	0.0024
Electrical conductivity	S/m	$5.5\cdot10^{-6}$	$3.46\cdot10^{6}$
Thermal conductivity	W/(m·°C)	0.606	16.5
Prandtl number	-	6.62	0.027

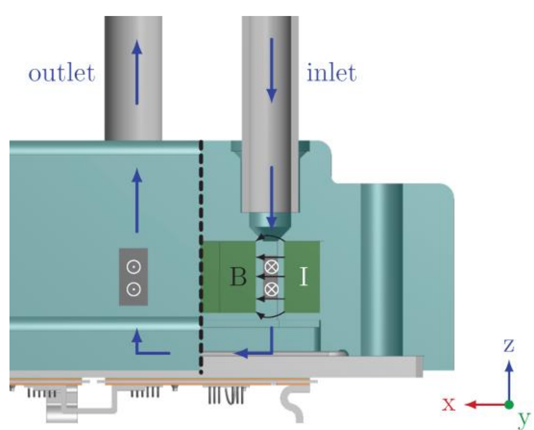

Fig. 9. Working principle of MHD liquid metal pump.

As Fig. 9 shows, because there is a constant magnetic field in ***x*** plane, injecting current through the electrodes in ***y*** plane, generates Lorentz force in ***z*** plane that is used for driving the conducting fluid in the channels of the pump. When a current is applied across the width of a channel filled with a conductive fluid subjected to an orthogonal magnetic field, the Lorentz force exerts body force on the fluid that is proportional to both the generated current density J in the fluid and the magnetic flux density B, as expressed in (2):

$$F = \int J \times B \cdot dV \approx B_{eff} I_{pump} L \tag{2}$$

where dV is the active volume of the pump, B_{eff} is the efficient magnetic flux density, I_{pump} is the current through the electrodes and L is the current flow distance between the two electrodes. Eq. (2) assumes that B and J are homogeneous and constant. The relationship between the pressure developed by the pump and mean velocity can be derived, as the flow in the system is pressure driven, shown in (3):

$$P_{MHD} = \frac{F}{A} \approx \frac{B_{eff} \cdot I_{pump}}{d} \approx C_1 \cdot \rho u^2 + C_2 \cdot \rho u \tag{3}$$

where P_{MHD} is the pressure developed by the pump and A is the cross section of the pump with length L and width d, u is the mean velocity across the channel, and finally, C_1 and C_2 are the coefficients of flow resistance through the system, considering pumps, piping and the tank of the loop. The flow rate across the pump, Q, can therefore be expressed as:

$$Q = uA = \left(\left({C_2}^2 + \frac{8 B_{eff} I_{pump} C_1}{\rho \pi r} \right)^{\frac{1}{2}} - C_2 \right) \cdot \frac{\pi r^2}{2 C_1} \tag{4}$$

where r is the radius of the tube and ρ is the fluid density. Eq. (4) shows a clear relationship between the flow rate Q and the applied current I_{pump}, which can be used to calculate the coolant's flow rate. In this work, coefficients C_1 and C_2 were determined by computational fluid dynamics (CFD) simulations, whereas B_{eff} was obtained empirically. Hence, for a specific current value, the flow rate can be predicted and applied in the CFD simulation to estimate the thermal characteristics of the liquid metal heat sink. The design parameters for the developed pump are shown in Table III and Fig. 10. The main disadvantage for implementing the proposed cooling scheme is the cost increase of the converter's thermal management that is mainly driven by the cost of the liquid metal, which is always more expensive compared to water even if mass-produced. However, substantial operational cost savings can be made with the proposed scheme as power modules will be utilized for a longer period. In addition the implementation of a liquid metal cooling system reduces the overall weight and volume of the cooling system significantly [31].

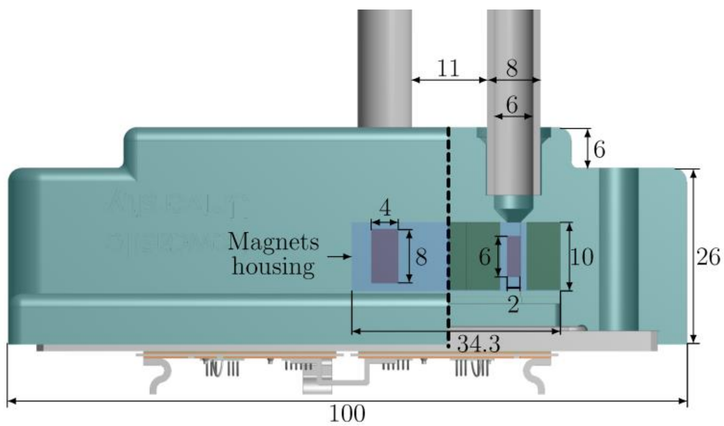

Fig. 10. Dimensions of the MHD pump in *mm* (front view).

TABLE III
LIQUID METAL MHD PUMP DESIGN PARAMETERS

Parameter	Symbol	Unit	Value
Cross sectional area of MHD channel	A	mm^2	2×10^1
Magnetic field cross sectional area	A_{mag}	mm^2	1×10^2
Efficient magnetic flux density	B_{eff}	T	0.3
Inner liquid metal pipe radius	r	mm	3
Channel distance between magnets	d	mm	2
Coefficient 1	C_1	-	6×10^{-4}
Coefficient 2	C_2	-	19×10^{-4}

Characterization of the pump for a range of input current values was also performed, in order to estimate B_{eff}, which is achieved by measuring the static pressure (P_s) for different current values. Once the pump is attached to the IGBT module, its slots and the piping system are filled with the liquid metal and positioned vertically. Then, a PWM controlled current, I_{pump}, is injected from a power supply unit (Agilent 6684A) to the pump's electrodes and the height difference (ΔH) between the inlet and outlet tubes is measured at the point where the liquid metal reaches its equilibrium position. Hence, in this position P_{MHD} equals the static pressure P_s, which can be defined as:

$$P_{MHD} = P_s = \rho g \Delta H \tag{5}$$

where g is the gravitational acceleration. In Fig. 11, the static pressure P_s is shown as a function of the supplied current I_{pump}. As expected, for a constant magnetic field, the static pump pressure varies linearly with the injected current. Therefore, B_{eff} is estimated by rearranging (3) and is shown in Table III.

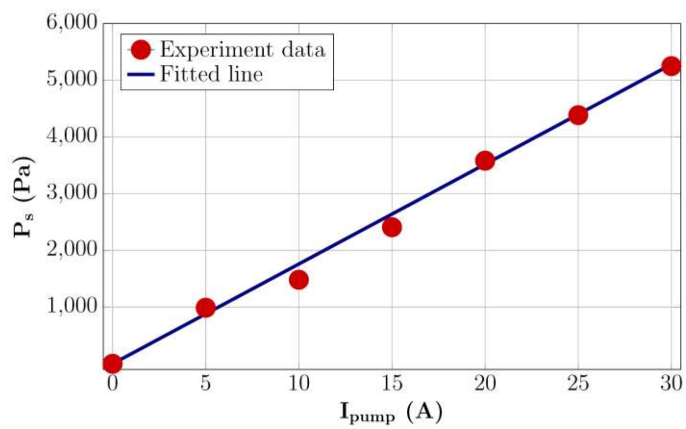

Fig. 11. MHD pump characterization: static pressure P_s as a function of input current I_{pump}

IV. EXPERIMENTAL TEST SETUP

A. Experimental Rig

A liquid metal-to-water heat exchanger is employed in this work for its power heat dissipation. The heat exchanger uses a U-shaped nickel pipe that accommodates the liquid metal and can be directly jointed with the inlet and outlet orifices of the MHD pump, although soft plastic connectors are used here for the ease of experimental connection. The heat exchanger pipe was made of nickel, as this material has high chemical resistivity against $Ga_{68}In_{22}Sn_{10}$.The pipe of the heat exchanger uses the same diameter as the inlet and outlet of the pump, in order to reduce the flow resistance in the loop. The slots of the MHD pump are the only points in the liquid metal loop that are narrower, in order to achieve high pressure for driving the coolant. The pipe is housed in an aluminum tank, which provides a water jacket from a liquid chiller unit (Cosmotec WRA70) with a predefined temperature. A flow meter (Q_w), pressure transducers ($P_{w\text{-}in}$ and $P_{w\text{-}out}$), and thermocouples ($T_{w\text{-}in}$, $T_{w\text{-}out}$, $T_{lm\text{-}in}$ and $T_{lm\text{-}out}$) are used for monitoring the water flow rate, the pressure drop across the heat exchanger and the inlet and outlet temperatures of water and liquid metal, respectively, as shown in Fig. 7. The liquid metal heat sink was subjected to both static and dynamic tests, to evaluate its cooling capability and its effectiveness in reducing the junction temperature fluctuations caused by load current changes. The schematic diagram of controlled load current and junction temperature measurement using a TSEP is shown in Fig. 12(a), whereas the experimental setup is presented in Fig. 12(b). The IGBT power module remains in its forward conducting state for the duration of the whole experiment, by applying a gate-emitter voltage of +15 V. A pulse DC current (I_{heat}), supplied by a TopCon Quadro programmable power supply unit, is emulating the heat losses ($P_{heat\ losses}$) produced by the IGBT chip.

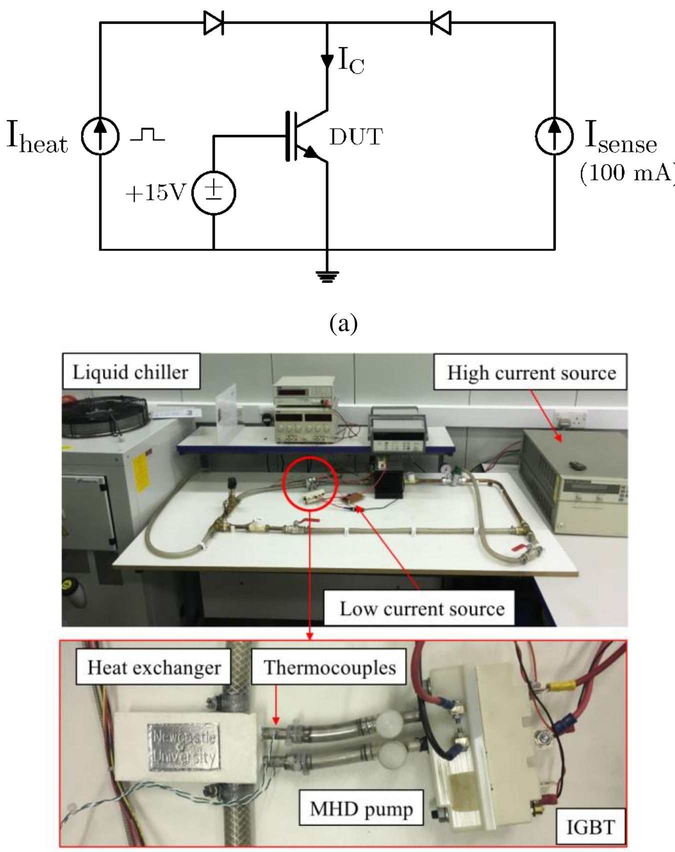

Fig. 12. Experimental setup: (a) Schematic diagram of IGBT heating and temperature sensing and (b) pictures of test bed

B. Junction Temperature Measurement

The chip junction temperature is required to evaluate the thermal properties of the heat sink. An indirect method via a TSEP was used for estimating the junction temperature. The temperature dependency of $V_{CE\text{-}on}$

on T_j for IGBTs at a low forward conduction current is obtained through a preliminary TSEP calibration test, where a hotplate was used to control the temperature of the IGBT chip externally. The TSEP calibration curve is shown in Fig. 13. A 100 mA sense current (I_{sense}) was selected in this study, as it provides high resolution (-2.14 mV/°C) without contributing to the self-heating of the IGBT device [7, 32]. For thermal characterization, the TSEP measurement takes place when the pulsed heating current I_{heat} is zero and only I_{sense} conducts. A dead time of 1 ms was added before measurement takes place in order to avoid measurement errors caused by the noise during the turn-off process. Then five consecutive $V_{CE\text{-}on}$ samples are obtained with a 10 µs delay between them. A median filter is therefore applied for the estimation of T_j. An example input waveform, used for both heating the IGBT and measuring T_j, is shown in Fig. 14.

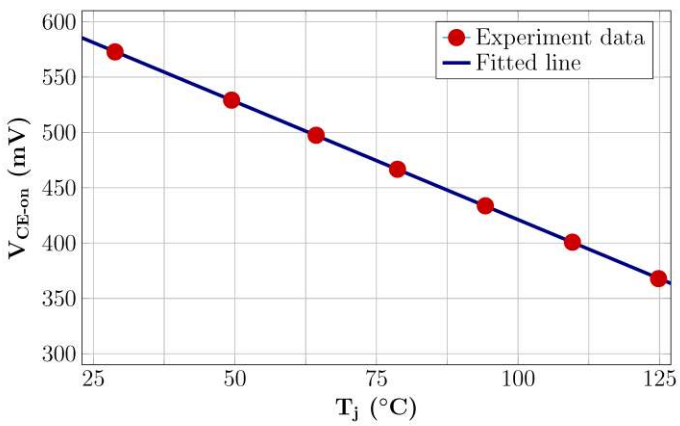

Fig. 13. TSEP calibration curve, showing the dependency of on-state voltage $V_{ce\text{-}on}$ on junction temperature T_j for 100 mA forward conducting current.

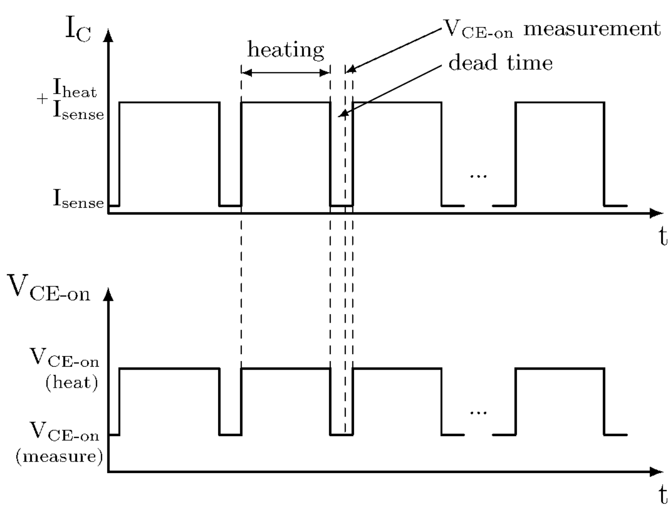

Fig. 14. Example waveform for IGBT heating and junction temperature measurement

C. Evaluation of the Cooling Capacity

It is essential to identify the cooling performance and heat dissipation capability of the liquid metal heat sink and to set boundaries in its operation. This was firstly evaluated with CFD simulations and verified with experimental results.

The conjugate heat transfer of MHD pump was simulated in ANSYS CFX 12.0, in which 3-D steady Reynolds-averaged Navier-Stokes (RANS) equations are solved for the fluid flow and energy equations are solved for fluid and solid simultaneously for the heat transfer. A few basic settings and assumptions are applied for the simulation i.e. (i) the flow is incompressible, (ii) the buoyancy and radiation heat transfer are not taken into account (iii) and the thermophysical properties of the liquid metal are temperature independent. The shear-stress-transport (SST) model is chosen as the turbulence model. Grid independence has also been examined, after which the grid of the solid domain has 111,292 nodes, and the grid of fluid domain has 195,245 nodes, which corresponds to a maximum y+ value of 1.0 on the wall boundary. Smooth wall conditions have been implemented over the wall. High resolution advection scheme is used too for the calculation of the advection terms, and root mean square residual of smaller than 10^{-5} is set as the convergence criterion. Results from the CFD analyses are shown in Fig. 15 and Fig 16. Fig. 15 represents the thermal characterization in a 3D plot for when the supplied pump current I_{pump} was varied between 0A and 15A and power losses $P_{heat\ losses}$ where varied between 0W and 40W. From Fig. 16 it can be concluded that the thermal resistance of the system is a function of the MHD pump's input current I_{pump}, as T_j steadily decreases with an increased current prior to 10 A. However, there is a marginal improvement on thermal conductivity when I_{pump} is higher than 10 A, suggesting the peak heat dissipation capability that will be discussed in the next sub-section.

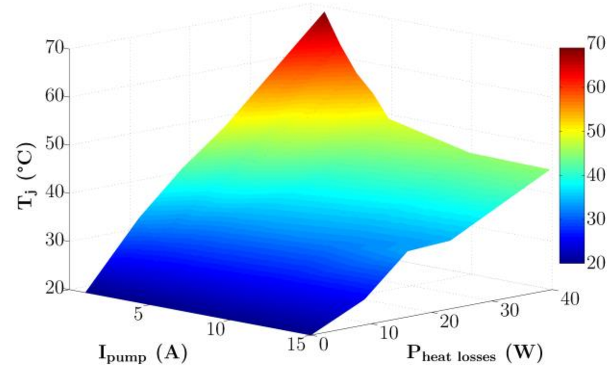

Fig. 15. Liquid metal heat sink characterization results

In the practical experiment the power losses $P_{heat\ losses}$ were obtained by multiplying collector current I_C and on-state voltage drop $V_{CE\text{-}on}$ during thermal equilibrium and T_j was measured during the low current interval. When the chip is subjected to a rising power loss ranging from 0 to 40 W, its junction temperature also increases. Experimental results are also shown in Fig. 16 for comparison and the experimental results matches the CFD simulation results.

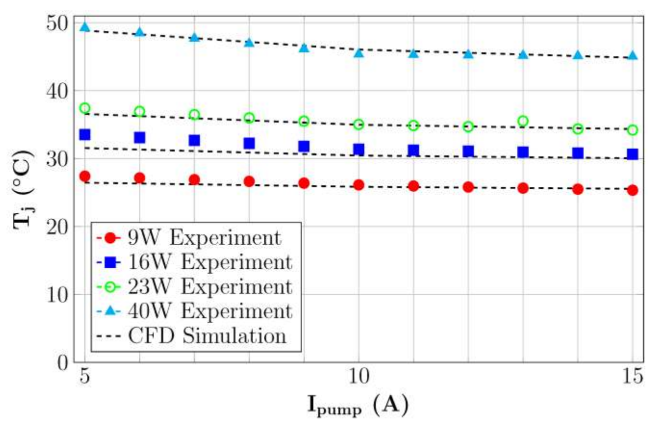

Fig. 16. CFD simulation and experimental results of liquid metal heat sink at various heat losses

D. MHD Pump Control

The dynamic thermal performance of the heat sink is evaluated for different values of I_{pump} and the system time constant (τ_{MHD}) is derived and illustrated in Fig. 17. As shown, the time required for the junction temperature, Tj to reach its steady state from a predefined temperature of 70°C is a function of I_{pump}. The time constant of the IGBT module is comparatively small and can be neglected. The results show that τ_{MHD} is dependent on the liquid metal flow rate, and therefore, the MHD pump current I_{pump}. Consequently, at higher input pump current, I_{pump}, heat in the baseplate is removed faster by the liquid metal coolant. For example, a

15A continuous pump current for 10s will bring the junction temperature into steady state. The relation between the time of heat removal τ_{MHD} and pump current is however exponential and not linear as shown in Fig. 17 and therefore requires a closed loop control. It should be noted that the glass transition temperature of the pump housing, T_g = 52ºC, cannot be exceeded. Otherwise, the thin nylon walls of the inlet and outlet slots in the liquid block could be damaged, as they are constantly subjected to the magnetic force generated by the embedded magnets of the MHD pump. Therefore, the characterization process for the current design was limited for junction temperatures ranging from 20 ºC to 70 ºC. At 70 ºC the liquid metal temperature is about 41 ºC which is below 52 ºC.

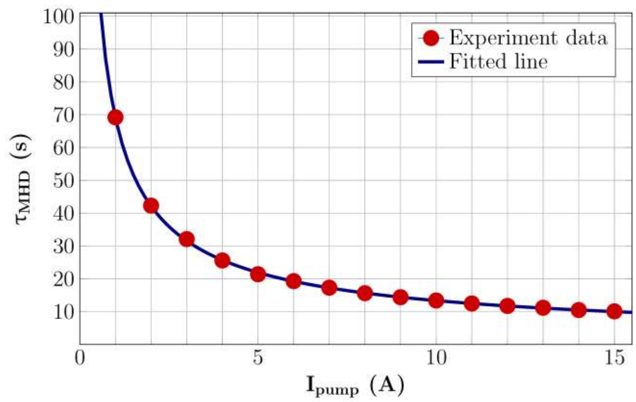

Fig. 17. MHD system time constant τ_{MHD} as a function of the pump current I_{pump}.

Fig. 18 shows the principal control structure for the junction temperature swing ΔT_j control experiment. The actual junction temperature (T_j^*) is measured with the help of the TSEP as indicated in Fig. 13. The obtained T_j^* value is compared to a reference value T_{ref} = 50 ºC and an error is generated. A proportional controller with k_p = 0.5 is used since the system has a very high time constant. Due to its high electric conductivity, the liquid metal between the electrodes form a current loop that has a rather small ohmic resistance (≈1mΩ) and therefore, very little power is required for driving the liquid metal as shown in Fig. 19. Thus, the electrodes of the MHD pump are connected to a variable controllable dc current source supply that can control the current of up to 15 A. A bench power supply (Agilent 6684A) was used as a current source for the MHD pump, which is a laboratory equipment and cannot be utilized in a real environment. A constant current source that is able to provide the maximum driving current of 15 A with a maximum efficiency of up to 90% can be used in a real application [33]. The pump current I_{pump} determines the flow rate Q of the liquid metal, which impinges against the baseplate and regulates junction temperature T_j^* at given power losses.

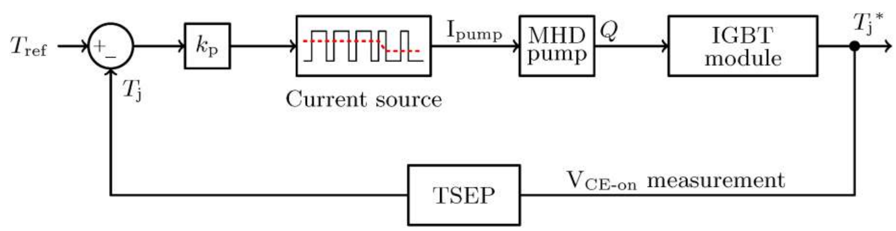

Fig. 18. Block diagram of liquid metal heat sink controller.

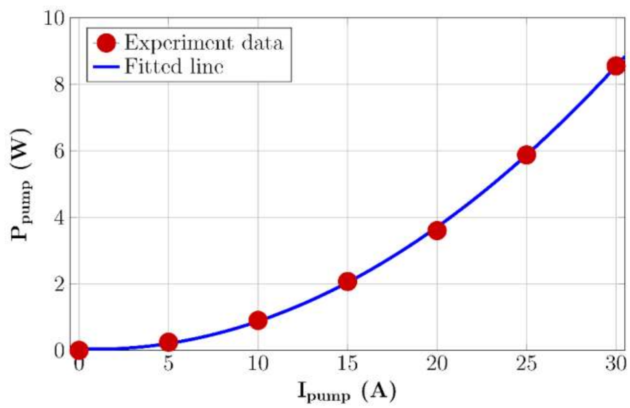

Fig. 19. Consumed power of liquid metal pump as a function of the input current.

V. Experimental Results

The effectiveness of the liquid metal heat sink in reducing ΔT_j is described in this Section. As already discussed, the mechanical load changes have a strong impact on the lifetime consumption of power semiconductor modules. The effectiveness of the proposed heat sink was tested by applying the metro-system mission profile mentioned previously in Section II. The scaled load current profile is presented in Fig. 20.

Two tests were conducted by subjecting the DUT to the same mission profile of Fig. 20; Test 1 - the MHD pump is fixed at a maximum cooling power powered from a constant I_{pump}=15 A current supply and Test 2 - the MHD pump is adaptively controlled with I_{pump} varying from 0A to a peak current up to 15A. Test 1 represents cooling to protect the IGBT device from thermal runaway and Test 2 represents cooling and junction temperature, T_j, control that aims to extend the lifetime of the power module by reducing ΔT_j. The results of both tests are shown in Fig. 21. In both experiments the water temperature was fixed at 20°C. The inlet liquid metal temperature, T_{lm}, has approximately the same value as water temperature due to the effective heat transfer properties of the heat exchanger.

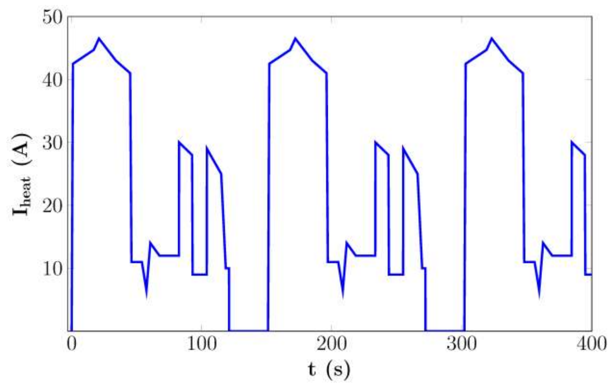

Fig. 20. Scaled metro load current mission profile

Fig. 20 shows that the junction temperature swing is greatly reduced with the introduction of the adaptive controller. The largest variations of the temperature are observed during accelerating and braking, as there is a large heat losses during these intervals. Similar to the simulation results, the temperature swing ΔT_j is reduced while the adaptive temperature controller is activated, in comparison to the case where maximum constant cooling is applied over the full metro-mission profile. The impact of the MHD time constant, τ_{MHD}, can be seen in Fig. 21 when compared with Fig. 6. The variation of the thermal resistance R_{th8} for the simulation model is instant, which results in fast changes of the junction temperature. For example, in Fig. 6 T_j is the same for both constant and adaptive cooling at the peak point, during the acceleration phase. On the other hand, during the experimental test there is a difference in the junction temperature T_j between the two cooling schemes during acceleration as a result of the time constant τ_{MHD} required by the heat sink to reach its steady state. The largest temperature swing occurs for both adaptive and constant cooling during the acceleration of the metro from a full stop to maximum speed. Over the course of a full metro cycle the adaptive cooling scheme manages to decrease the maximum ΔT_j's from 31°C to 19°C, which corresponds to a 12°C decrease between the two cooling methods. As a consequence, the mean junction temperature is increased by 8°C, which also contributes to the IGBT lifetime consumption, but as previously mentioned, its impact is not as strong as the temperature fluctuation [4]. Also in Fig. 21, the supplied pump current for each case is shown. With the thermal controller activated, the pump current is constantly changing, which affects the flow rate of the liquid metal and therefore, the thermal resistance of the system. Fig. 21 shows that the average current required by the adaptive cooling scheme is 50% smaller compared to the uncontrolled cooling which decreases the power consumption of the MHD pump.

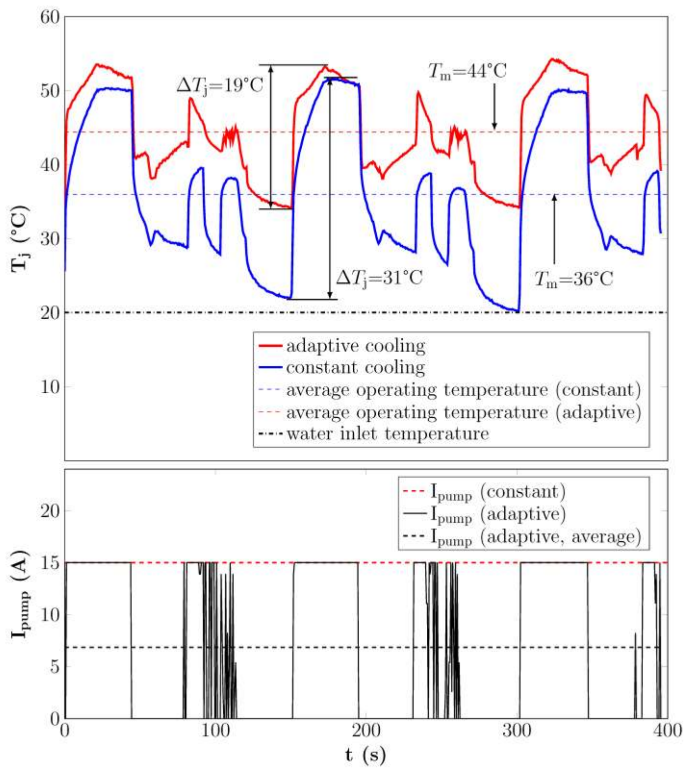

Fig. 20. Junction temperature, T_j, results and liquid metal pump supplied current, I_{pump}, with and without thermal controller.

VI. Conclusion

This work presented an active liquid metal cooled heat sink, designed to reduce the temperature swing of the junction temperature in order to increase the lifetime of power modules. A magnetohydrodynamic (MHD) pump, which has no rotating components and thus is simple, reliable and easy to control, was designed to impinge liquid metal against the baseplate of the power module. Both pump and IGBT module form one unit. The pump is controlled by using a simple P-controller that controls the amount of current that flows through the liquid metal in order to generate the exact pump power. As the cooling flow rate is actively changed, the heat flux from the chip to the baseplate is controlled and therefore the junction temperature can be influenced. Simulation and experimental results have been conducted. The highest temperature swing observed for constant cooling is 31ºC, whereas it is reduced to 19ºC by implementing the adaptive cooling. Hence, the proposed cooling method achieves a ΔT_j reduction of 12ºC. The paper also presents the design of an MHD pump which becomes an integral part of the power module.

ACKNOWLEDGEMENTS

This work was sponsored by Vehicle Electrical Systems Integration (VESI) project (EP/I038543/1), which is funded by the Engineering and Physical Sciences Research Council (EPSRC).

REFERENCES

[1] B. Wang, J. Cai, X. Du, and L. Zhou, "Review of power semiconductor device reliability for power converters," *CPSS Transactions on Power Electronics and Applications,* vol. 2, pp. 101-117, 2017.

[2] Y. Liu, M. Huang, H. Wang, X. Zha, J. Gong, and J. Sun, "Reliability-Oriented Optimization of the LC Filter in a Buck DC-DC Converter," *IEEE Transactions on Power Electronics,* vol. 32, pp. 6323-6337, 2017.

[3] S. Yang, D. Xiang, A. Bryant, P. Mawby, L. Ran, and P. Tavner, "Condition Monitoring for Device Reliability in Power Electronic Converters: A Review," *IEEE Transactions on Power Electronics,* vol. 25, pp. 2734-2752, 2010.

[4] M. Held, P. Jacob, G. Nicoletti, P. Scacco, and M. H. Poech, "Fast power cycling test of IGBT modules in traction application," in *Power Electronics and Drive Systems, 1997. Proceedings., 1997 International Conference on*, 1997, pp. 425-430 vol.1.

[5] R. Bayerer, T. Herrmann, T. Licht, J. Lutz, and M. Feller, "Model for Power Cycling lifetime of IGBT Modules - various factors influencing lifetime," in *Integrated Power Systems (CIPS), 2008 5th International Conference on*, 2008, pp. 1-6.

[6] B. Ji, V. Pickert, B. Zahawi, and M. Zhang, "In-situ bond wire health monitoring circuit for IGBT power modules," in *Power Electronics, Machines and Drives (PEMD 2012), 6th IET International Conference on*, 2012, pp. 1-6.

[7] B. Ji, X. Song, W. Cao, V. Pickert, Y. Hu, J. W. Mackersie*, et al.*, "*In Situ* Diagnostics and Prognostics of Solder Fatigue in IGBT Modules for Electric Vehicle Drives," *Power Electronics, IEEE Transactions on,* vol. 30, pp. 1535-1543, 2015.

[8] M. Andresen, K. Ma, G. Buticchi, J. Falck, F. Blaabjerg, and M. Liserre, "Junction temperature control for more reliable power electronics," *IEEE Transactions on Power Electronics,* vol. PP, pp. 1-1, 2017.

[9] E. Laloya, L. Ó, H. Sarnago, and J. M. Burdío, "Heat Management in Power Converters: From State of the Art to Future Ultrahigh Efficiency Systems," *IEEE Transactions on Power Electronics,* vol. 31, pp. 7896-7908, 2016.

[10] I. Mudawar, D. Bharathan, K. Kelly, and S. Narumanchi, "Two-phase spray cooling of hybrid vehicle electronics," in *Thermal and Thermomechanical Phenomena in Electronic Systems, 2008. ITHERM 2008. 11th Intersociety Conference on*, 2008, pp. 1210-1221.

[11] P. Wang, P. McCluskey, and A. Bar-Cohen, "Two-Phase Liquid Cooling for Thermal Management of IGBT Power Electronic Module," *Journal of Electronic Packaging,* vol. 135, pp. 021001-021001, 2013.

[12] A. J. Robinson, "A Thermal-Hydraulic Comparison of Liquid Microchannel and Impinging Liquid Jet Array Heat Sinks for High-Power Electronics Cooling," *Components and Packaging Technologies, IEEE Transactions on,* vol. 32, pp. 347-357, 2009.

[13] L. Yonglu, L. Xiaobing, and L. Wei, "Experimental Research on a Honeycomb Microchannel Cooling System," *Components, Packaging and Manufacturing Technology, IEEE Transactions on,* vol. 1, pp. 1378-1386, 2011.

[14] P. R. Parida, S. V. Ekkad, and K. Ngo, "Multi-Layer Mini-Channel and Ribbed Mini-Channel Based High Performance Cooling Configurations for Automotive Inverters—Part A: Design and Evaluation," *Journal of Thermal Science and Engineering Applications,* vol. 5, pp. 031010-031010, 2013.

[15] Y. Deng and J. Liu, "Optimization and Evaluation of a High-Performance Liquid Metal CPU Cooling Product," *Components, Packaging and Manufacturing Technology, IEEE Transactions on,* vol. 3, pp. 1171-1177, 2013.

[16] Y. Deng and J. Liu, "Design of Practical Liquid Metal Cooling Device for Heat Dissipation of High Performance CPUs," *Journal of Electronic Packaging,* vol. 132, pp. 031009-031009, 2010.

[17] U. Ghoshal, D. Grimm, S. Ibrani, C. Johnston, and A. Miner, "High-performance liquid metal cooling loops," in *Semiconductor Thermal Measurement and Management Symposium, 2005 IEEE Twenty First Annual IEEE*, 2005, pp. 16-19.

[18] Y. Deng and J. Liu, "A liquid metal cooling system for the thermal management of high power LEDs," *International Communications in Heat and Mass Transfer,* vol. 37, pp. 788-791, 2010.

[19] J. Vetrovec, D. A. Copeland, R. Feeler, and J. Junghans, "Testing of active heat sink for advanced high-power laser diodes," in *SPIE LASE*, 2011, pp. 79180G-79180G-6.

[20] M. Tawk, Y. Avenas, A. Kedous-Lebouc, and M. Petit, "Numerical and Experimental Investigations of the Thermal Management of Power Electronics With Liquid Metal Mini-Channel Coolers," *Industry Applications, IEEE Transactions on,* vol. 49, pp. 1421-1429, 2013.

[21] J. Vetrovec, "High-Performance Heat Sink for Hybrid Electric Vehicle Inverters," in *ASME 2010 International Design Engineering Technical Conferences and Computers and Information in Engineering Conference*, 2010, pp. 235-240.

[22] W. Xiang, W. Yun, and A. Castellazzi, "Reduced active and passive thermal cycling degradation by dynamic active cooling of power modules," in *Power Semiconductor Devices & IC's (ISPSD), 2015 IEEE 27th International Symposium on*, 2015, pp. 309-312.

[23] W. Xiang, A. Castellazzi, and P. Zanchetta, "Temperature control for reduced thermal cycling of power devices," in *Power Electronics and Applications (EPE), 2013 15th European Conference on*, 2013, pp. 1-10.

[24] L. Cong, J. Da, J. Jizhou, G. Feng, and W. Jin, "Thermoelectric Cooling for Power Electronics Circuits: Modeling and Active Temperature Control," *Industry Applications, IEEE Transactions on,* vol. 50, pp. 3995-4005, 2014.

[25] X. Zhang and L.-D. Zhao, "Thermoelectric materials: Energy conversion between heat and electricity," *Journal of Materiomics,* vol. 1, pp. 92-105, 2015/06/01/ 2015.

[26] M. Ke, M. Liserre, F. Blaabjerg, and T. Kerekes, "Thermal Loading and Lifetime Estimation for Power Device Considering Mission Profiles in Wind Power Converter," *Power Electronics, IEEE Transactions on,* vol. 30, pp. 590-602, 2015.

[27] W. Lai, M. Chen, L. Ran, O. Alatise, S. Xu, and P. Mawby, "Low ΔTj Stress Cycle Effect in IGBT Power Module Die-Attach Lifetime Modeling," *IEEE Transactions on Power Electronics,* vol. 31, pp. 6575-6585, 2016.

[28] Y. Deng and J. Liu, "Hybrid liquid metal–water cooling system for heat dissipation of high power density microdevices," *Heat and Mass Transfer,* vol. 46, pp. 1327-1334, December 01 2010.

[29] B. Ji, "In-situ health monitoring of IGBT power modules in EV applications," 2012.

[30] X. Perpiñà, L. Navarro, X. Jordà, M. Vellvehi, J.-F. Serviere, and M. Mermet-Guyennet, "Reliability and Lifetime Prediction for IGBT Modules in Railway Traction Chains."

[31] M. Musallam, C. Yin, C. Bailey, and M. Johnson, "Mission Profile-Based Reliability Design and Real-Time Life Consumption Estimation in Power Electronics," *IEEE Transactions on Power Electronics,* vol. 30, pp. 2601-2613, 2015.

[32] Y. Avenas, L. Dupont, and Z. Khatir, "Temperature Measurement of Power Semiconductor Devices by Thermo-Sensitive Electrical Parameters—A Review," *IEEE Transactions on Power Electronics,* vol. 27, pp. 3081-3092, 2012.

[33] TDK-Lambda. 175/180/200W Configurable ac/dc power supply - NV-Power NV-175. *NV175 69530-Rev 25.*